

# Ultra-long magnetization needle induced by focusing azimuthally polarized beams with a spherical mirror

LI HANG<sup>1</sup>, KAI LUO<sup>1</sup>, JIAN FU<sup>1</sup>, YIZHE CHANG<sup>1</sup>, YING WANG<sup>1</sup>, AND PEIFENG CHEN<sup>1\*</sup>

<sup>1</sup> School of Optical and Electronic Information, Huazhong University of Science and Technology(HUST), 1037 Luoyu Road Wuhan 430074, China

\*Corresponding author: pfchen@hust.edu.cn

Compiled January 30, 2018

Based on extended Richards-Wolf theory for axisymmetric surfaces and the inverse Faraday effect, we propose the generation of a purely longitudinal magnetization needle by focusing Gaussian annular azimuthally polarized beams with a spherical mirror. The needle obtained has a longitudinal length varying hundreds to thousands of wavelengths with keeping the lateral size under  $0.4\lambda$ , and the corresponding aspect ratio can easily reach more than 2000. It may be the first time that a magnetization needle whose aspect ratio is over 500 is achieved. The approximate analytical expressions of the magnetization needle are given and the longitudinal length is tunable by changing the value of the angular thickness and position of the annular beams. © 2018 Optical Society of America

**OCIS codes:** (160.3820) Magneto-optical materials; (050.1960) Diffraction theory; (260.5430) Polarization.

<http://dx.doi.org/10.1364/ao.XX.XXXXXX>

## 1. INTRODUCTION

Interaction between laser and magneto-optical materials has aroused hot interest over a few years. Different kinds of magnetization fields, such as magnetization needles [1–6], magnetization chains [6–8], magnetization spots arrays [9, 10] and other magnetization fields [11] can be realized. Specially, purely longitudinal magnetization needles, magnetization fields with extensive longitudinal size and small lateral size, play an important role in many applications such as data storage, spin wave operations, ferromagnetic semiconductor devices, and particle manipulation [12–15]. To further promote these practical applications, including increasing the density of magnetic storage and producing magnetic lattices for atomic trap, it is required to improve the aspect ratio (AR) of the magnetization needles while keeping that their lateral size is sub-wavelength. Based on the inverse Faraday effect (IFE) in magneto-optic (MO) films, pure longitudinal magnetization needles can be obtained by focusing azimuthally polarized vortex beams (APVBs) in recent researches. The magnetization needles in most works have the longitudinal full width at half maximums (LFWHMs) less than  $30\lambda$  and corresponding ARs are difficult to beyond 100 [1–4].

Recently, Yan et al. achieved a magnetization needle with  $107\lambda$  depths and  $0.37\lambda$  lateral size by using a multi-zone plate phase filter [5]. The AR reaches up to 289. However, these studies have mainly concentrated on aplanatic systems and complex phase modulation. The larger AR is, the more sophisticated phase plates are. The phase plates in the literature [5] are very complex and difficult to manufacture. It seems that AR is nearly impossible to further improve by using aplanatic systems. On the contrary, optical needles whose LFWHMs reach  $1000\lambda$  can be realized by using reflectors with spherical aberration [16, 17]. Therefore, a sphere mirror, instead of an aplanatic system, is used in this paper to achieve hundreds to thousands of wavelengths magnetization needles in longitudinal length and their ARs can easily reach over 2000.

This paper is organized as follows. In Section 2, magnetization field induced by focusing azimuthally polarized beams with a sphere mirror is calculated based on extended Richards-Wolf theory and the IFE. Approximate analytical expressions of magnetization needles are given. In Section 3, LFWHMs and the transverse full width at half maximums (TFWHMs) of the magnetization needles are discussed. In Section 4, we conclude our work.

## 2. THEORY AND CONFIGURATION

Fig. 1 shows the geometry of a spherical mirror illuminated by an annular azimuthally polarized beam (APB). A spiral phase plate (SPP) is front of the mirror. The SPP is a phase modulator that delays the phase of the incident beam from 0 to  $2n\pi$ , and its transmittance function is  $T(\varphi) = \exp(in\varphi)$  when its topological charge is  $n$ . A magneto-optic film with IFE is located at the "focal line", where a magnetization needle will generate.

Calculating magnetization needle fields needs a diffraction integral, but an analysis based on geometrical optics can help to understand how a spherical mirror extends LFWHM of a magnetization needle. As shown in Fig. 1, every ray of light crosses  $z$ -axis at a different position. Therefore, the position of every ray and the full width of the incident beam can be represented by angle  $\alpha_0$  and  $\Delta\alpha$ , respectively. If the central ray is located at  $\alpha_0$ , according to geometrical optics, the length of the "focal line" is

$$\Delta z \approx \frac{\Delta\alpha R \sin \frac{\alpha_0}{2}}{4 \cos^2 \frac{\alpha_0}{2}} (\Delta\alpha \ll \alpha_0), \quad (1)$$

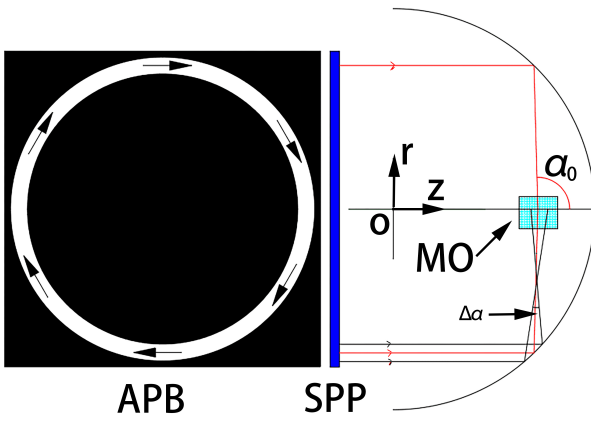


**Fig. 1.** Diagram of an annulus of light incident on a spherical mirror centered on O. APB is a narrow annular Gaussian azimuthally polarized beam. SPP (blue rectangle) denotes a spiral phase plate, and MO (cyan rectangle) is a magneto-optic film.  $\alpha_0$  and  $\Delta\alpha$  represent the position and the thickness of the incident APB, respectively. The system is azimuthally symmetric.

where  $R$  is the radius of the mirror. It is noted that the approximation in Eq. (1) is also not right when  $\Delta\alpha$  is too small, because diffraction will be intense and geometrical optics will fail. To make a more precise result, diffraction should be considered.

According to extended Richards-Wolf theory [18], the electric field near the focus of an APVB can be expressed as [6]

$$\vec{E}(r, \phi, z) = \begin{bmatrix} E_r \\ E_\phi \\ E_z \end{bmatrix} = Ai^m e^{im\phi} \begin{bmatrix} I_{m-1} + I_{m+1} \\ i(I_{m-1} - I_{m+1}) \\ 0 \end{bmatrix}, \quad (2)$$

with

$$I_n(r, z) = \int_{\alpha_{min}}^{\alpha_{max}} l(\alpha) q(\alpha) J_n(kr \sin \alpha) \times \sin \alpha \exp(i\Phi) d\alpha, \quad (3)$$

where  $A$ , which will be omitted in the following, is a constant related to wavelength  $\lambda$ ,  $k = 2\pi/\lambda$  is wave number and  $m$  is the topological charge of the SPP. The function  $q(\alpha)$  is apodization factor, obtained from energy conservation. For a spherical mirror,  $q(\alpha) = 1$  [18]. The function  $l(\alpha)$  is the amplitude distribution of the incident beam and  $J_n$  denotes the  $n$ th-order Bessel function of the first kind. For an aplanatic system, the phase term  $\Phi = kz \cos \alpha$ . As for a spherical mirror, the corrective phase term is [17, 18]

$$\Phi = k[z \cos \alpha - 2R \cos(\alpha/2)]. \quad (4)$$

Based on IFE, the induced magnetization field is expressed as

$$\vec{M} = i\gamma \vec{E} \times \vec{E}^*, \quad (5)$$

where  $\gamma$ , which will be omitted in the following, is the magneto-optic constant,  $\vec{E}^*$  is conjugate of the electric field  $\vec{E}$ . Substituting Eqs. (2)~(4) to Eq. (5), the magnetization field can be expressed as

$$\vec{M} = M(r, z) \vec{e}_z = 2(|I_{m-1}|^2 - |I_{m+1}|^2) \vec{e}_z. \quad (6)$$

Eq. (6) shows that the magnetization field is purely longitudinal because the focal electric field is purely transverse. If a Gaussian annulus of light is used as an incident beam, the function  $l(\alpha)$  is expressed as

$$l(\alpha) = \exp[-(\alpha - \alpha_0)^2 / \Delta\alpha^2]. \quad (7)$$

Eqs. (4) and (7) provide that a strong oscillation occurs in the phase term and the only significant contribution to the integral arises from the position near  $\alpha_0$ . Through an asymptotic approximation when  $\Delta\alpha^2 k R \gg 1$  [17], the magnetization field can be approximately expressed as

$$M(r, z) \approx 4\pi l^2 \sin^2(\alpha_s) (J_{m-1}^2 - J_{m+1}^2) / |\Phi''(\alpha_s)|, \quad (8)$$

where  $l = l(\alpha_s)$ ,  $J_n = J_n(kr \sin \alpha_s)$ .  $\alpha_s$  is stationary phase angle, i.e.  $\Phi'(\alpha_s) = 0$ . When the surface accuracy of the spherical mirror is considered, an additional phase  $\phi(\alpha, \beta)$  should be added in Eq. (4), where  $\beta$  is azimuthal angle. If  $\phi(\alpha, \beta)$  is constant, the stationary phase angle  $\alpha_s$  will not change so a perfect magnetization needle can still form. If  $\phi(\alpha, \beta)$  is only independent of  $\beta$ , Eq. (8) is still suitable. As long as  $\frac{d\phi}{d\alpha}$  is not too large, the magnetization needle can generate normally but an analytical result cannot be obtained. If  $\phi(\alpha, \beta)$  is dependent on  $\beta$ , the symmetry of the magnetization needle will be destroyed. In the following, only the ideal situation is considered.

If  $\Delta\alpha \ll \alpha_0$ ,  $\alpha_s$  can be expanded around  $\alpha_0$ ,

$$\alpha_s \approx \alpha_0 + (z - z_0) \frac{4 \cos^2 \frac{\alpha_0}{2}}{R \sin \frac{\alpha_0}{2}}, \quad (9)$$

where  $z_0 = \frac{R}{2 \cos \frac{\alpha_0}{2}}$ . Utilizing Eq. (9), Eq. (8) can be further approximately expressed as

$$M(r, z) \approx \frac{4\pi \sin^2(\alpha_0)}{|\Phi''(\alpha_0)|} \exp\left[-\frac{16(z - z_0)^2 \cos^4(\alpha_0/2)}{\Delta\alpha^2 R^2 \sin^2(\alpha_0/2)}\right] \times (J_{m-1}^2(kr \sin \alpha_0) - J_{m+1}^2(kr \sin \alpha_0)). \quad (10)$$

### 3. DISCUSSION

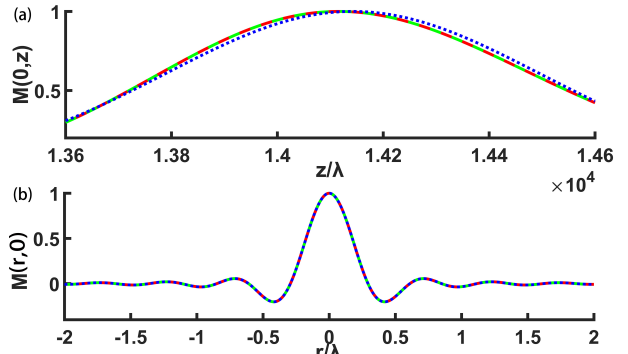


**Fig. 2.** Normalized magnetization distribution along  $z$ -axis and  $r$ -axis with  $\alpha_0 = \pi/2$ ,  $\Delta\alpha = 0.1$ ,  $m = 1$ , and  $R = 20000\lambda$ . Fig. 2(a) is the longitudinal magnetization profile and Fig. 2(b) is the transverse magnetization profile. The solid red line is generated from Eqs. (2)~(7) with  $\alpha_{min} = \alpha_0 - 3\Delta\alpha$  and  $\alpha_{max} = \alpha_0 + 3\Delta\alpha$ ; the dashed green line is produced by Eq. (8); the dotted blue line corresponds to Eq. (10).

Fig. 2 shows that an axial profile at  $r = 0$  and a lateral profile at  $z = 0$  of a magnetization needle by three methods. It is displayed that the magnetization field is like a non-diffracting beam whose LFWHM is about  $800\lambda$  (in Fig. 2(a)) with lateral size beyond diffraction limit (in Fig. 2(b)). The solid red line is generated from Eqs. (2)~(7) by numerical integration; the dashed green line is produced by asymptotic approximation Eq. (8); the dotted blue line corresponds to Gaussian approximation Eq. (10). The method from numerical integration can be regarded as a standard result. Three methods lead to a consistent result in Fig. 2(b) but not a perfect one in Fig. 2(a), because the stationary phase angle  $\alpha_s$  is independent of  $r$  but dependent on  $z$ . The asymptotic approximation has some deviations compared with the Gaussian approximation but little difference with the numerical integration in Fig. 2(a). However, if  $\Delta\alpha$  becomes smaller, difference between the asymptotic approximation and the numerical integration will gradually arise and the asymptotic approximation will gradually become inaccurate. On the contrast, difference between the asymptotic approximation and the Gaussian approximation will gradually vanish when  $\Delta\alpha$  decreases, which is yet meaningless because the sole value of the Gaussian approximation is to estimate LFWHMs and they are inaccurate compared with the numerical method if  $\Delta\alpha$  is too small. In spite of the deviations, it is still suitable to estimate the LFWHM of the needle by using the Gaussian approximation. The LFWHM is the distance of the two roots of the equation  $M(r, z)/M(r, z_0) = 1/2$ . With the help of Eq. (10), it can be approximately expressed as

$$\text{LFWHM} \approx \frac{(2 \ln 2)^{1/2} \Delta\alpha R \sin \frac{\alpha_0}{2}}{4 \cos^2 \frac{\alpha_0}{2}}. \quad (11)$$

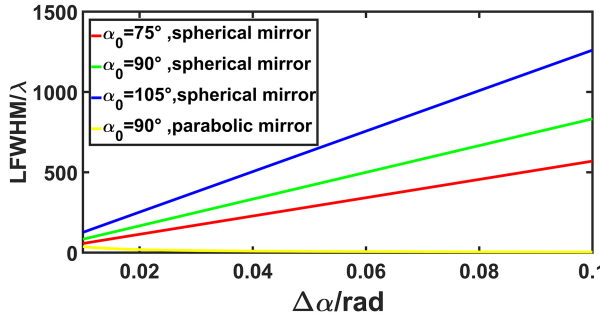


**Fig. 3.** LFWHM vs  $\Delta\alpha$  with  $R = 20000\lambda$  (except the yellow line). The red line is for  $\alpha_0 = 75^\circ$ ; the green line is for  $\alpha_0 = 90^\circ$ ; the blue line is for  $\alpha_0 = 105^\circ$ . These three lines are generated from Eq. (11). The yellow line is for  $\alpha_0 = 90^\circ$  with a parabolic mirror, which is generated from [6] or [19].

This result is the same as Eq. (1), since the full width at half maximum of the incident beam by Eq. (7) is  $(2 \ln 2)^{1/2} \Delta\alpha$ . The more interesting finding is that Eq. (11) is consistent with the length of the optical needle by focusing radially polarized beam in [17]. It is proved that the method to extend LFWHM is independent of the polarization of incident beams. Furthermore, Eq. (11) shows that LFWHM is proportional to spherical radius  $R$  and the angular width  $\Delta\alpha$ , which is displayed in Fig. 3. In addition, it is increasing with the angular position  $\alpha_0$ . Therefore,  $\alpha_0$  is expected to be larger when a bigger LFWHM is desired. Besides, some practical applications may be restricted when  $\alpha_0 < 90^\circ$  because the magnetization needle is generated by a beam retro-reflected toward the inner cavity of the spherical

mirror, which can be avoided when  $\alpha_0 > 90^\circ$  as long as an annular spherical mirror is used to replace a spherical mirror.

Compared with the LFWHM at  $\alpha_0 = 75^\circ$ , it increases by 120% at  $\alpha_0 = 105^\circ$ . When  $\Delta\alpha = 0.1$  and  $R = 20000\lambda$ , the LFWHM is about  $833\lambda$  for  $\alpha_0 = 90^\circ$  and about  $1260\lambda$  for  $\alpha_0 = 105^\circ$  as shown in Fig. 3, which is much larger than [1–6]. As for a needle generated from a parabolic mirror, the LFWHM is under  $40\lambda$  when the angular width  $\Delta\alpha$  varies from  $0.01\text{rad}$  to  $0.1\text{rad}$  as shown in Fig. 3. If we want to get the same LFWHM ( $833\lambda$ ) with a parabolic mirror at the same numerical aperture (NA), the angular width  $\Delta\alpha$  should be under  $4.5 \times 10^{-4}\text{rad}$  when NA=1 (i.e.  $\alpha_0 = 90^\circ$ ) [6, 19], which is too thin to realize. A detailed comparison between a spherical mirror and a parabolic mirror is described in [17].

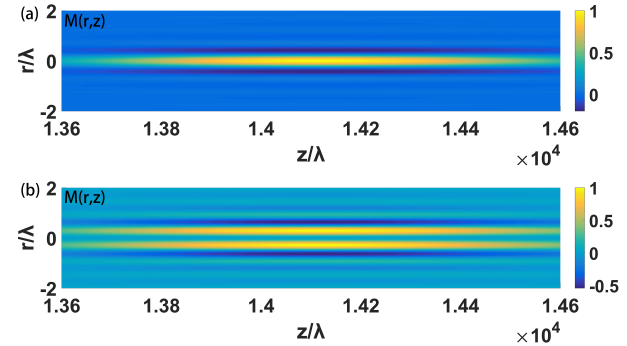


**Fig. 4.** Normalized magnetization distribution in  $r$ - $z$  plane with  $\alpha_0 = \pi/2$ ,  $\Delta\alpha = 0.1$ , and  $R = 20000\lambda$ . (a) A magnetization needle for  $m=1$ . (b) A magnetization needle with dual channels for  $m=2$ . This figure is generated from Eq. (8).

Fig. 4 displays that a magnetization needle with a single channel for  $m = 1$  and a magnetization needle with dual channels for  $m = 2$ . It is indicated that their LFWHMs are equal but TFWHMs are different. For the needle of a single channel with  $m = 1$ , the maximum is at  $r = 0$ . Solving the equation  $M(r, z)/M(0, z) = 1/2$  by Eq. (10), it is obtained that  $\text{TFWHM} \approx 0.3498\lambda / \sin \alpha_0$  as shown in Fig. 5 and corresponding AR is

$$AR \approx \frac{1.683 \Delta\alpha R \sin^2 \frac{\alpha_0}{2}}{\lambda \cos \frac{\alpha_0}{2}}. \quad (12)$$

Fig. 5 shows that the TFWHM is symmetric with respect to  $\alpha_0 = 90^\circ$ . The minimum TFWHM is at  $\alpha_0 = 90^\circ$  while AR increases with  $\alpha_0$  because the LFWHM increases with  $\alpha_0$ . It should be pointed that AR is a significant parameter for magnetization needles. In this paper, when  $\Delta\alpha = 0.1$  and  $R = 20000\lambda$ , the AR is about 2380 with  $\alpha_0 = 90^\circ$ , 7.2 times larger than 289 in [5]. Moreover, the system in this paper is much easier to realize.

Similarly, it is calculated that the TFWHM for  $m = 2$  is about  $0.2717\lambda / \sin \alpha_0$  and corresponding AR is about 29% larger than the AR for  $m = 1$ .

Fig. 4 presents that lateral size of the needles is almost constant along  $z$ -axis, but an analytical result is more convincing. Solving the equation  $M(r, z)/M(0, z) = 1/2$  with  $m = 1$  by Eq. (8), it is obtained that  $\text{TFWHM} \approx 0.3498\lambda / \sin \alpha_s$ . Fig. 6 shows that TFWHMs vary along  $z$ -axis with three different  $\alpha_0$ . At  $\alpha_0 = 90^\circ$ , the TFWHM and its variation are both minimum. It is also concluded that the TFWHMs are under  $0.375\lambda$  when  $\alpha_0$  varies from  $75^\circ$  to  $105^\circ$  in the focal region. As for the needles of dual channels, the result is similar.

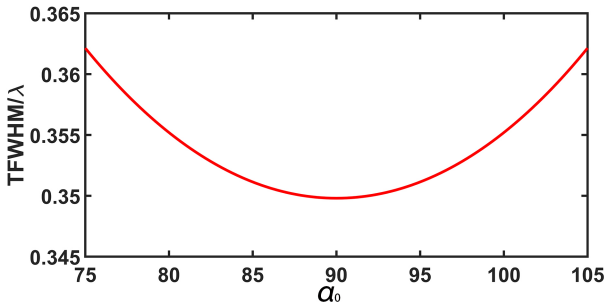


**Fig. 5.** TFWHM vs  $\alpha_0$  for  $m = 1$ .  $\alpha_0$  varies from  $75^\circ$  to  $105^\circ$ .

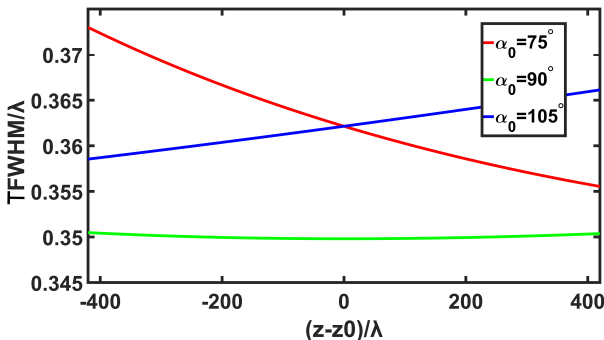


**Fig. 6.** TFWHMs vary along  $z$ -axis with  $\Delta\alpha = 0.1$  and  $R = 20000\lambda$ . This figure is generated from Eq. (8).

#### 4. CONCLUSION

In conclusion, we theoretically proposed the generation of purely longitudinal magnetization needle by focusing a Gaussian annulus of APVBs with a spherical mirror. The longitudinal size is tunable from hundreds to thousands of wavelengths by changing the angular width and position. Meanwhile, the lateral size is under  $0.375\lambda$  in a large dynamic range. The AR in this paper can be easily over 2000 while previous work was far smaller than 1000. The ultra-long magnetization needle with sub-wavelength scale can play a significant role in all-optical magnetic recording, atomic trapping, confocal and magnetic resonance microscopy.

#### REFERENCES

- Y. Jiang, X. Li, and M. Gu, "Generation of sub-diffraction-limited pure longitudinal magnetization by the inverse faraday effect by tightly focusing an azimuthally polarized vortex beam," *Opt. Lett* **38**, 2957–2960 (2013).
- S. Wang, X. Li, J. Zhou, and M. Gu, "Ultralong pure longitudinal magnetization needle induced by annular vortex binary optics," *Opt. Lett* **39**, 5022–5025 (2014).
- W. Ma, D. Zhang, L. Zhu, and J. Chen, "Super-long longitudinal magnetization needle generated by focusing an azimuthally polarized and phase-modulated beam," *Chin. Opt. Lett* **13**, 052101 (2015).
- W. Yan, Z. Nie, X. Zhang, Y. Wang, and Y. Song, "Magnetization shaping generated by tight focusing of azimuthally polarized vortex multi-gaussian beam," *Appl. Opt.* **56**, 1940–1946 (2017).
- W. Yan, Z. Nie, X. Zhang, Y. Wang, and Y. Song, "Generation of an ultralong pure longitudinal magnetization needle with high axial homogeneity using an azimuthally polarized beam modulated by pure multi-zone plate phase filter," *J. Opt.* **19**, 085401 (2017).
- W. Yan, Z. Nie, X. Zhang, Y. Wang, and Y. Song, "Theoretical guideline for generation of an ultralong magnetization needle and a super-long conveyed spherical magnetization chain," *Opt. Express* **25**, 22268–22279 (2017).
- Z. Nie, W. Ding, D. Li, X. Zhang, Y. Wang, and Y. Song, "Spherical and sub-wavelength longitudinal magnetization generated by  $4\pi$  tightly focusing radially polarized vortex beams," *Opt. Express* **23**, 690–701 (2015).
- Z. Nie, W. Ding, G. Shi, D. Li, X. Zhang, Y. Wang, and Y. Song, "Achievement and steering of light-induced sub-wavelength longitudinal magnetization chain," *Opt. Express* **23**, 21296–21305 (2015).
- Z.-Q. Nie, H. Lin, X.-F. Liu, A.-P. Zhai, Y.-T. Tian, W.-J. Wang, D.-Y. Li, W.-Q. Ding, X.-R. Zhang, Y.-L. Song, and B.-H. Jia, "Three-dimensional super-resolution longitudinal magnetization spot arrays," *Light: Science & Applications* **6**, e17032 (2017).
- C. Hao, Z. Nie, H. Ye, H. Li, Y. Luo, R. Feng, X. Yu, F. Wen, Y. Zhang, C. Yu, J. Teng, B. Luk'yanchuk, and C.-W. Qiu, "Three-dimensional supercritical resolved light-induced magnetic holography," *Sci. Adv.* **3**, e1701398 (2017).
- S. Wang, Y. Cao, and X. Li, "Generation of uniformly oriented in-plane magnetization with near-unity purity in  $4\pi$  microscopy," *Opt. Lett.* **23**, 5050–5053 (2017).
- S. Y. Chou, M. S. Wei, P. R. Krauss, and P. B. Fischer, "Single-domain magnetic pillar array of 35 nm diameter and 65 gbits/in.2 density for ultrahigh density quantum magnetic storage," *J. Appl. Phys.* **76**, 6673–6675 (1994).
- S. A. Nikitov, P. Tailhades, and C. S. Tsai, "Spin waves in periodic magnetic structures/magnonic crystals," *J. Magn. Magn. Mater* **236**, 320–330 (2001).
- D. Chiba, M. Sawicki, Y. Nishitani, Y. Nakatani, F. Matsukura, and H. Ohno, "Magnetization vector manipulation by electric fields," *Nature* **455**, 515–518 (2008).
- S. N. Atutov, R. Calabrese, V. Guidi, B. Mai, A. G. Ru-davets, E. Scansani, L. Tomassetti, V. Biancalana, A. Burchiantica, C. Marinelli, E. Mariotti, L. Moi, and S. Vero-nesi, "Fast and efficient loading of a rub magneto-optical trap using light-induced atomic desorption," *Phys. Rev. A* **67**, 053401 (2003).
- L. Hang, Y. Wang, and P. Chen, "Needles of light produced with a quasi-parabolic mirror," *J. Opt. Soc. Am. A* **35**, 174–178 (2018).
- D. Panneton, G. St-Onge, M. Piché, and S. Thibault, "Needles of light produced with a spherical mirror," *Opt. Lett* **40**, 419–422 (2015).
- D. Panneton, G. St-Onge, M. Piché, and S. Thibault, "Exact vectorial model for nonparaxial focusing by arbitrary axisymmetric surfaces," *J. Opt. Soc. Am. A* **33**, 801–810 (2016).
- H. Dehez, A. April, and M. Piché, "Needles of longitudinally polarized light: guidelines for minimum spot size and tunable axial extent," *Opt. Express* **20**, 14891–14905 (2012).